

Pinning down the leptophobic Z' in leptonic final states with Deep Learning

Tanumoy Mandal,^{1,*} Aniket Masaye,¹ Subhadip Mitra,^{2,†} Cyrin Neeraj,^{2,‡} Naveen Reule,^{1,§} and Kalp Shah^{2,¶}

¹Indian Institute of Science Education and Research Thiruvananthapuram, Vithura, Kerala, 695 551, India

²Center for Computational Natural Sciences and Bioinformatics,

International Institute of Information Technology, Hyderabad 500 032, India

(Dated: September 27, 2023)

A leptophobic Z' that does not couple with the Standard Model leptons can evade the stringent bounds from the dilepton-resonance searches. In our earlier paper [T. Arun *et al.*, Search for the Z' boson decaying to a right-handed neutrino pair in leptophobic $U(1)$ models, *Phys. Rev. D*, **106** (2022) 095035; arXiv:2204.02949], we presented two gauge anomaly-free $U(1)$ models—one based on the Green-Schwarz (GS) anomaly cancellation mechanism, and the other on a grand unified theory (GUT) framework with gauge kinetic mixing—where a heavy leptophobic Z' is present along with right-handed neutrinos (N_R). We pointed out the interesting possibility of a correlated search for Z' and N_R at the LHC through the $pp \rightarrow Z' \rightarrow N_R N_R$ channel. This channel can probe a part of the Z' parameter space beyond the reach of the standard dijet resonance searches. In this follow-up paper, we analyse the challenging monolepton final state arising from the decays of the N_R pair with Deep Learning. We present the high-luminosity LHC discovery reaches for six different GUT embeddings and a benchmark point in the GS setup. We also update our previous estimates in the dilepton channel with Deep Learning. We identify parameter regions that can be probed with the proposed channel but will remain inaccessible to dijet searches at the HL-LHC.

I. INTRODUCTION

Many extensions of the Standard Model (SM), like the grand unified theories (GUTs) [1–3], contain an electrically neutral colour-singlet heavy gauge boson, Z' . To get such a particle in the spectrum in a bottom-up manner, one can simply add an extra local $U(1)$ symmetry spontaneously broken by a complex scalar field with a TeV-scale vacuum expectation value (vev). The phenomenology of a TeV-scale Z' is well-explored in the literature (see, e.g., [4, 5]). One of the current programs of the LHC is to look for the signature of Z' . However, so far, the focus has been only on the cases where it decays exclusively to the SM particles [6–14]. The failure to find the Z' so far motivates us to look for other possibilities with *nonstandard* decay modes of Z' , i.e., where it can decay to beyond-the-SM (BSM) particles as well.

The strongest exclusion limits on the Z' parameter space usually come from the dilepton resonance searches [8, 9]. For instance, the current mass exclusion limit on a sequential Z' is about 5 TeV [8]. The stringent dilepton exclusion limits can be evaded if the Z' is leptophobic, i.e., it does not couple (or couples very feebly) to the SM leptons. In the leptophobic case, the nonstandard decay modes of the Z' can become important as the branching ratios (BRs) to the new modes can be high. One interesting possibility is when the Z' decays to a pair of right-handed neutrinos (RHNs, N_R) [15–20]. While appending an additional $U(1)$ gauge symmetry to the SM group, one must ensure

the cancellation of all gauge anomalies to maintain gauge invariance and renormalizability of the theory. To cancel the gauge anomalies, one can include RHNs in the particle spectrum [21] or rely on some special mechanism like the Green-Schwarz (GS) mechanism [22, 23]. The minimal GS mechanism does not require RHNs. However, the cancellation of pure gravity anomaly motivates the existence of RHNs. Therefore, many anomaly-free $U(1)$ extensions of the SM contain RHNs since they can also help generate light neutrino masses through various seesaw mechanisms.

In our previous paper [24], we presented two theoretically well-motivated leptophobic Z' scenarios where the Z' dominantly decays to a pair of RHNs. Being leptophobic, these scenarios can easily bypass the dilepton exclusion limits. At the same time, a large BR of the $Z' \rightarrow N_R N_R$ decay and the subsequent decays of N_R to $W\ell$, $Z\nu$, and $H\nu$ final states open up many interesting leptonic final states (see, e.g., Fig. 1). The process $pp \rightarrow Z' \rightarrow N_R N_R$ is important not only from the Z' -search point of view but also for the RHN searches. Since RHNs are SM singlets, producing them at the LHC is difficult as their production cross sections are small, suppressed by the light-heavy neutrino mixing angles. However, they can be copiously produced if they come from the decays of another BSM particle [25–28].

We considered the $pp \rightarrow Z' \rightarrow N_R N_R$ channel in a leptophobic setup in Ref. [24]. We studied the dilepton channel (which is easy to analyse with a cut-based analysis and shows a good sensitivity) to estimate the HL-LHC reach. Interestingly, we found that a large chunk of the parameter space beyond the reach of $pp \rightarrow Z' \rightarrow jj$ can be probed through this channel at the HL-LHC. The decay of the RHN pair can lead to multilepton final states. The monolepton mode is complimentary but more challenging because of the difficulty in the background reduction. In this follow-up paper, we estimate the reach in the monolepton final

* tanumoy@iisertvm.ac.in

† subhadip.mitra@iiit.ac.in

‡ cyrin.neeraj@research.iiit.ac.in

§ naveenreule20@iisertvm.ac.in

¶ kalp.shah@research.iiit.ac.in

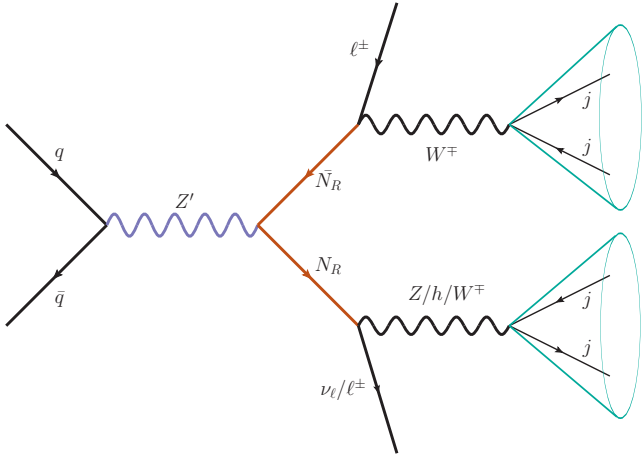


FIG. 1. Representative Feynman diagram for a leptophobic Z' decaying to two right-handed neutrinos.

state with a deep neural network (DNN) model.

The RHNs we consider are around the TeV scale, much lighter than the standard type-I seesaw scale $\sim 10^{14}$ GeV. To naturally realise the TeV-scale RHNs, we consider inverse-seesaw mechanism (ISM) for neutrino mass generation [29, 30]. As a result, unlike the Majorana-type RHNs in the type-I seesaw, the RHNs here are pseudo-Dirac in nature. If neutrino mass is generated using a type-I seesaw mechanism, because of the Majorana nature of the RHNs, the collider consequences will be different from the ISM. For example, from the $pp \rightarrow Z' \rightarrow N_R N_R$ process, we get a same-sign dilepton signature, which is not present in the ISM framework. Earlier, in Refs. [31–35], different $U(1)$ extensions using the ISM were considered in various contexts. Also, the future lepton colliders could be the best testing ground for the heavy neutrinos [36–38].

The rest of the paper is organised as follows. In Sec. II, we review the leptophobic models; in Sec. III, we present our analysis of the monolepton channel; in Sec. IV, we estimate the HL-LHC prospects of the monolepton channel. We also update our estimate of the dilepton prospects with the DNN in Sec. V. Finally, we conclude in Sec. VI.

II. LEPTOPHOBIC Z' MODELS

We look at the two examples of anomaly-free gauge extensions of the SM from Ref. [24], where a leptophobic Z' with substantial $Z' \rightarrow N_R N_R$ branchings is present. In one example, the RHNs cancel the mixed gauge-gravity anomaly while the GS mechanism cancels the rest. In the other example, the leptophobia of Z' arises in a GUT framework [39–42]. Below, we briefly review the essential details of these two constructions and elaborate on some aspects for completeness.

TABLE I. Particle representations and quantum numbers in the GS anomaly-cancellation setup.

	$SU(3)_c$	$SU(2)_L$	$U(1)_Y$	$U(1)_z$
Q_L	3	2	1/3	z_q
u_R	$\bar{\mathbf{3}}$	1	4/3	αz_q
d_R	$\bar{\mathbf{3}}$	1	-2/3	βz_q
ℓ_L	1	2	-1	0
e_R	1	1	-2	0
N_R	1	1	0	z_N
H	1	2	1	0
ϕ	1	1	0	1
S_L	1	1	0	0

A. Leptophobia with GS mechanism

In this model, the particle spectrum includes three RHNs (one for every generation) equally charged under the extra $U(1)_z$. Even though the RHNs are not essential for gauge anomaly cancellation with the GS mechanism [23], the cancellation of the pure gravity anomaly motivates us to introduce them. The light-neutrino masses are generated through the ISM, which requires an extra chiral sterile fermion S_L per generation.

We show the $U(1)_z$ charges of various particles in Table I. The SM leptons are uncharged under $U(1)_z$ to make the Z' leptophobic. The nonzero $U(1)_z$ charges of the quarks ensure that the Z' can be produced at the LHC through quark-quark fusion. The $U(1)_z$ charge assignment is generation-independent, and we introduce two free parameters α and β to parametrise the right-handed up and down-type quark charges, respectively ($\alpha = \beta = -1$ in Ref. [24]). The SM Higgs doublet is chargeless under $U(1)_z$ to minimise the mixing between Z and Z' . The scalar ϕ with unit $U(1)_z$ charge is the flavon field needed to generate the quark Yukawa interactions as shown in Eq. (5). The fermion masses arise after ϕ and H get vacuum expectation values.

The charge assignment in Table I leads to six anomalous triangle diagrams proportional to the traces of the product of the generators:

1. $[SU(3)_C]^2[U(1)_z]$: $\text{tr}[\{\mathcal{T}^a, \mathcal{T}^b\}_z] = 3z_q(2 - \alpha - \beta)$,
2. $[SU(2)_L]^2[U(1)_z]$: $\text{tr}[\{T^a, T^b\}_z] = 6z_q$,
3. $[U(1)_z]^3$: $\text{tr}[z^3] = 3z_q^3(2 - \alpha^3 - \beta^3) - z_N^3$,
4. $[U(1)_Y]^2[U(1)_z]$: $\text{tr}[Y^2 z] = \frac{2z_q}{3}(1 - 8\alpha - 2\beta)$,
5. $[U(1)_Y][U(1)_z]^2$: $\text{tr}[Y z^2] = 2z_q^2(1 - 2\alpha^2 + \beta^2)$,
6. $[R]^2[U(1)_z]$: $\text{tr}[z] = 3z_q(2 - \alpha - \beta) - z_N$.

Since gravity becomes prominent at high scales, it is natural to assume that the mixed gauge-gravity anomaly vanishes at low energy without the GS mechanism. Therefore,

we set

$$3z_q(2 - \alpha - \beta) - z_N = 0 \quad (1)$$

by hand. This gives us a relation between the $U(1)_z$ charges of the quarks and RHNs.

To cancel the other anomalies with the GS mechanism [43, 44], we add new gauge-dependent terms in the Lagrangian with carefully chosen coefficients. The Peccei-Quinn (PQ) terms for the mixed gauge anomalies and the $[U(1)_z]^3$ anomaly can be written as

$$\begin{aligned} \mathcal{L}_{\text{PQ}} = & \frac{1}{96\pi^2} \left(\frac{\Theta}{M} \right) \varepsilon_{\mu\nu\rho\sigma} \left[g_z^2 \mathcal{C}_{zzz} F_z^{\mu\nu} F_z^{\rho\sigma} + g_z g' \mathcal{C}_{zzy} F_z^{\mu\nu} F_Y^{\rho\sigma} \right. \\ & + g'^2 \mathcal{C}_{zYY} F_Y^{\mu\nu} F_Y^{\rho\sigma} + g^2 \mathcal{D}_2 \text{tr} (F_W^{\mu\nu} F_W^{\rho\sigma}) \\ & \left. + g_S^2 \mathcal{D}_3 \text{tr} (F_S^{\mu\nu} F_S^{\rho\sigma}) \right]. \quad (2) \end{aligned}$$

Under the new $U(1)_z$, the pseudoscalar (Goldstone) axion Θ transforms as $\Theta \rightarrow \Theta + M g_z \theta_z$ and the new gauge field transforms as $B_z^\mu \rightarrow B_z^\mu - \partial^\mu \theta_z$. Here, M is the scale at which $U(1)_z$ breaks through the Stückelberg mechanism, F_z, F_Y, F_W, F_S are the field strengths and g_z, g', g, g_S are the coupling constants associated with the $U(1)_z, U(1)_Y, SU(2)_L, SU(3)_c$ gauge groups, respectively. The generalised Chern-Simons (GCS) terms for other mixed anomalies are given as

$$\begin{aligned} \mathcal{L}_{\text{GCS}} = & \frac{1}{48\pi^2} \varepsilon_{\mu\nu\rho\sigma} \left[g'^2 g_z \mathcal{C}_{zYY} B_Y^\mu B_z^\nu F_Y^{\rho\sigma} + g' g_z^2 \mathcal{C}_{zzy} B_Y^\mu B_z^\nu F_z^{\rho\sigma} \right. \\ & \left. + g^2 g_z \mathcal{K}_2 B_z^\mu \Omega_W^{\nu\rho\sigma} + g_S^2 g_z \mathcal{K}_3 B_z^\mu \Omega_S^{\nu\rho\sigma} \right] \quad (3) \end{aligned}$$

with

$$\begin{aligned} \Omega_{S,W}^{\nu\rho\sigma} = & \frac{1}{3} \text{tr} \left[A_{S,W}^\nu \left(F_{S,W}^{\rho\sigma} - [A_{S,W}^\rho, A_{S,W}^\sigma] \right) \right. \\ & \left. + (\text{cyclic permutations of } \rho, \sigma, \nu) \right] \end{aligned}$$

and $A_X = [G, W]$. The coefficients $\mathcal{C}, \mathcal{D}, \mathcal{E}$, and \mathcal{K} can be solved in terms of the $U(1)_z$ charges of the fermions as

$$\begin{aligned} \mathcal{C}_{zzz} &= -3z_q^3 (2 - \alpha^3 - \beta^3) + z_N^3, \\ \mathcal{C}_{zYY} &= 2z_q (2\beta - 8\alpha - 1) = \frac{3}{2} \mathcal{C}_{zYY}, \\ \mathcal{C}_{zzy} &= 6z_q (2\alpha^2 - \beta^2 - 1) = 3\mathcal{E}_{zzy}, \\ \mathcal{D}_2 &= -18z_q = -\frac{3}{2} \mathcal{K}_2, \\ \mathcal{D}_3 &= 9z_q (\alpha + \beta - 2) = -\frac{3}{2} \mathcal{K}_3, \end{aligned} \quad (4)$$

to cancel the anomalies. The $U(1)_z$ invariant Yukawa interactions are written as

$$\mathcal{L}_Y \supset -\lambda_u \left(\frac{\phi}{\Lambda} \right)^{2z_q} \bar{Q}_L \tilde{H} u_R - \lambda_d \left(\frac{\phi}{\Lambda} \right)^{2z_q} \bar{Q}_L H d_R + h.c., \quad (5)$$

where $\tilde{H} = i\sigma_2 H^*$, and λ_u and λ_d are the Yukawa couplings. After the spontaneous breaking of the $U(1)_z$ symmetry, ϕ acquires a vev, $v_\phi = \langle \phi \rangle$, leading to the SM Yukawa terms. We set $z_q = 1/2$ for our analysis. This fixes $z_N = 6$ for $\alpha = \beta = -1$.

1. Neutrino mass generation

The neutrino masses are generated by the ISM through the following higher-dimensional operators,

$$\begin{aligned} \mathcal{L}_Y \supset & -\lambda_{ij}^v \left(\frac{\phi^\dagger}{\Lambda} \right)^{z_N} \bar{L}_L^i \tilde{H} N_R^j - M_{Rij} \left(\frac{\phi}{\Lambda} \right)^{z_N} \bar{N}_R^i S_L^j \\ & - \frac{\mu}{2} \bar{S}_L^c S_L + h.c. \quad (6) \end{aligned}$$

We get the mass matrix for the neutrinos after the sequential breaking of the $U(1)_z$ and electroweak symmetries in the $(\nu_L^c N_R S_L^c)^T$ basis as,

$$\mathbf{M}_\nu = \begin{pmatrix} 0 & \mathbf{m}_D & 0 \\ \mathbf{m}_D^T & 0 & \mathbf{M}_R \\ 0 & \mathbf{M}_R^T & \mu \end{pmatrix}, \quad (7)$$

where $\mathbf{m}_D = \lambda^v v_h$, μ , and \mathbf{M}_R are 3×3 mass matrices in the generation space in general. The parameter μ is typically associated with lepton number violation and restores the lepton number symmetry in the $\mu \rightarrow 0$ limit. After diagonalising the matrix in Eq. (7), we get the active (light) neutrino mass matrix as [45],

$$\mathbf{m}_\nu = \mathbf{m}_D \mathbf{M}_R^{-1} \mu (\mathbf{M}_R^T)^{-1} \mathbf{m}_D + \mathcal{O} \left(\mu \frac{\mathbf{m}_d^4}{\mathbf{M}_R^4} \right). \quad (8)$$

There is a double suppression of the light neutrino masses from the large \mathbf{M}_R (taken around the TeV scale) and the small μ .

B. Leptophobia in E_6 GUT models

A leptophobic Z' can be realised in some E_6 GUT models through gauge-boson kinetic mixing [39] even though the fermion couplings to the gauge bosons are not arbitrary free parameters. The $U(1)_z$ group in such models can come from a symmetry-breaking chain, like,

$$\begin{aligned} E_6 &\rightarrow SO(10) \times U(1)_\chi \\ &\rightarrow SU(5) \times U(1)_\chi \times U(1)_\psi \\ &\rightarrow SU(2)_L \times U(1)_Y \times U(1)_z \\ &\rightarrow SU(2)_L \times U(1)_Y. \end{aligned} \quad (9)$$

The fundamental representation of E_6 is **27** dimensional, containing all the SM fermions along with two colour-neutral isosinglets ν^c and $\tilde{\nu}^c$, a colour-singlet isodoublet $\mathcal{L} = (N E)^T$ and its conjugate \mathcal{L}^c , and a colour-triplet isosinglet \mathcal{D} and its antiparticle \mathcal{D}^c . The RHN can be identified with either ν^c or $\tilde{\nu}^c$. Under $SO(10)$, the **27** dimensional representation breaks into a **16**, a **10** and an **1**. These further break into representations of $SU(5)$. In the *standard* embedding (I in Table II), we put all the SM fermions and the RHN into the **16**, and the new fermions in the **10** and the **1**. There are five other ways one can embed these fermions,

TABLE II. Quantum numbers ($\overline{Q}_\psi \equiv 2\sqrt{6}Q_\psi$, $\overline{Q}_\chi \equiv 2\sqrt{10}Q_\chi$) of the particle contained in the **27** representation of E_6 for the six possible embeddings—the first one is called the standard embedding. Here, $\mathcal{G}_{\text{SM}} \equiv SU(3)_c \times SU(2)_L \times U(1)_Y$. The $\tan\theta$ and δ values needed to get the *leptophobic* Z' boson in each embedding are shown in the bottom rows.

Particle	\mathcal{G}_{SM}	I		II		III		IV		V		VI	
		\overline{Q}_ψ	\overline{Q}_χ										
$Q = (u, d)^T$	$(\mathbf{3}, \mathbf{2})_{1/3}$	1	-1	1	-1	1	-1	1	-1	1	-1	1	-1
$L = (\nu, e)^T$	$(\mathbf{1}, \mathbf{2})_{-1}$	1	3	-2	-2	1	3	-2	-2	1	3	-2	-2
u^c	$(\overline{\mathbf{3}}, \mathbf{1})_{-4/3}$	1	-1	1	-1	1	3	1	3	-2	-2	-2	-2
d^c	$(\overline{\mathbf{3}}, \mathbf{1})_{2/3}$	1	3	1	3	1	-1	1	-1	1	-1	1	-1
e^c	$(\mathbf{1}, \mathbf{1})_2$	1	-1	1	-1	1	-5	1	-5	4	0	4	0
ν^c	$(\mathbf{1}, \mathbf{1})_0$	1	-5	1	-5	1	-1	1	-1	1	-1	1	-1
$\mathcal{L} = (N, E)^T$	$(\mathbf{1}, \mathbf{2})_{-1}$	-2	-2	1	3	-2	-2	1	3	-2	-2	1	3
$\mathcal{L}^c = (N^c, E^c)^T$	$(\mathbf{1}, \mathbf{2})_1$	-2	2	-2	2	-2	2	-2	2	-2	2	-2	2
\mathcal{D}	$(\mathbf{3}, \mathbf{1})_{-2/3}$	-2	2	-2	2	-2	2	-2	2	-2	2	-2	2
\mathcal{D}^c	$(\overline{\mathbf{3}}, \mathbf{1})_{2/3}$	-2	-2	-2	-2	-2	-2	-2	-2	1	3	1	3
$\tilde{\nu}^c$	$(\mathbf{1}, \mathbf{1})_0$	4	0	4	0	4	0	4	0	1	-5	1	-5
$\tan\theta$		$\sqrt{3/5}$		$\sqrt{3/5}$		$\sqrt{15}$		$\sqrt{5/27}$		$\sqrt{5/3}$		0	
δ		-1/3		-1/3		$-\sqrt{10}/3$		$-\sqrt{5/12}$		$-\sqrt{5/12}$		$-\sqrt{10}/3$	

leading to a total of six different embeddings [42]. In Table II, we show the new charges of all the fermions for the six different embeddings.

From the chain in Eq. (9), the $U(1)_z$ charge Q_z can be expressed as $Q_z = Q_\psi \cos\theta - Q_\chi \sin\theta$ where θ is the E_6 mixing angle. However, there is no solution for θ where the lepton- Z' couplings vanish. Therefore, we look at the $U(1)_Y \leftrightarrow U(1)_z$ gauge-kinetic mixing terms allowed by the gauge invariance,

$$\mathcal{L}_{\text{kin}} \supset -\frac{1}{4}\tilde{F}_Y^{\mu\nu}\tilde{F}_{Y\mu\nu} - \frac{1}{4}\tilde{F}_z^{\mu\nu}\tilde{F}_{z\mu\nu} - \frac{\sin\chi}{2}\tilde{F}_Y^{\mu\nu}\tilde{F}_z^{\mu\nu}. \quad (10)$$

The kinetic mixing, parametrised by $\sin\chi$, can be removed by the following transformation [41]:

$$\tilde{B}_Y^\mu = B_Y^\mu - \tan\chi B_z^\mu, \quad \tilde{B}_z^\mu = \frac{B_z^\mu}{\cos\chi}. \quad (11)$$

However, this cancellation is valid only at a particular scale, implying that the mixing term can regenerate at higher orders. This makes the couplings energy-dependent. Hence, they must be evaluated at the TeV scale before relating to the experiments. After the above rotation, the couplings of the abelian gauge bosons with the fermions are given as [41],

$$\mathcal{L}_{\text{int}} \supset -\bar{\psi}\gamma_\mu \left[g' \frac{Y}{2} B_Y^\mu + g_z \left(Q_z + \sqrt{\frac{3}{5}} \delta \frac{Y}{2} \right) B_z^\mu \right] \psi, \quad (12)$$

where $\delta = -\tilde{g}_Y \sin\chi / \tilde{g}_z$. Now, the fermion couplings are functions of two free parameters θ and δ ; we can, in general, make the couplings of any two fields vanish. For example, for the *standard* embedding (Table II), leptophobia

TABLE III. Effective $U(1)_z$ charges for various E_6 embeddings and the GS model. For the six E_6 embeddings, we compute the charges using the leptophobic $\tan\theta$ and δ combinations from Table II. For the GS model, we use the benchmark point mentioned in Sec. II A.

Model	z_u	z_d	z_N
<i>E₆ embedding</i>			
I	1.242	0.786	-1.667
II	1.242	0.786	-1.667
III	0.393	0.248	-0.527
IV	0.962	0.481	-1.936
V	0.481	0.481	-1.936
VI	0.393	0.248	-0.527
GS	0.707	0.707	6

corresponds to $\theta = \tan^{-1} \sqrt{3/5}$ and $\delta = -1/3$ [42]. Different combinations of θ and δ work in different embeddings, as shown in Table II.

III. COLLIDER ANALYSIS

For collider analysis, we use the following simplified Lagrangian,

$$\mathcal{L} \supset \frac{g_z}{2} (z_u \bar{u}_i \gamma^\mu u_i + z_d \bar{d}_i \gamma^\mu d_i + z_N \bar{N}_R \gamma^\mu N_R) Z'_\mu, \quad (13)$$

where $z_{u,d}$ are the effective $U(1)_z$ charges of up and down type quarks (for any quark q , $z_q^2 = z_{qL}^2 + z_{qR}^2$). We show

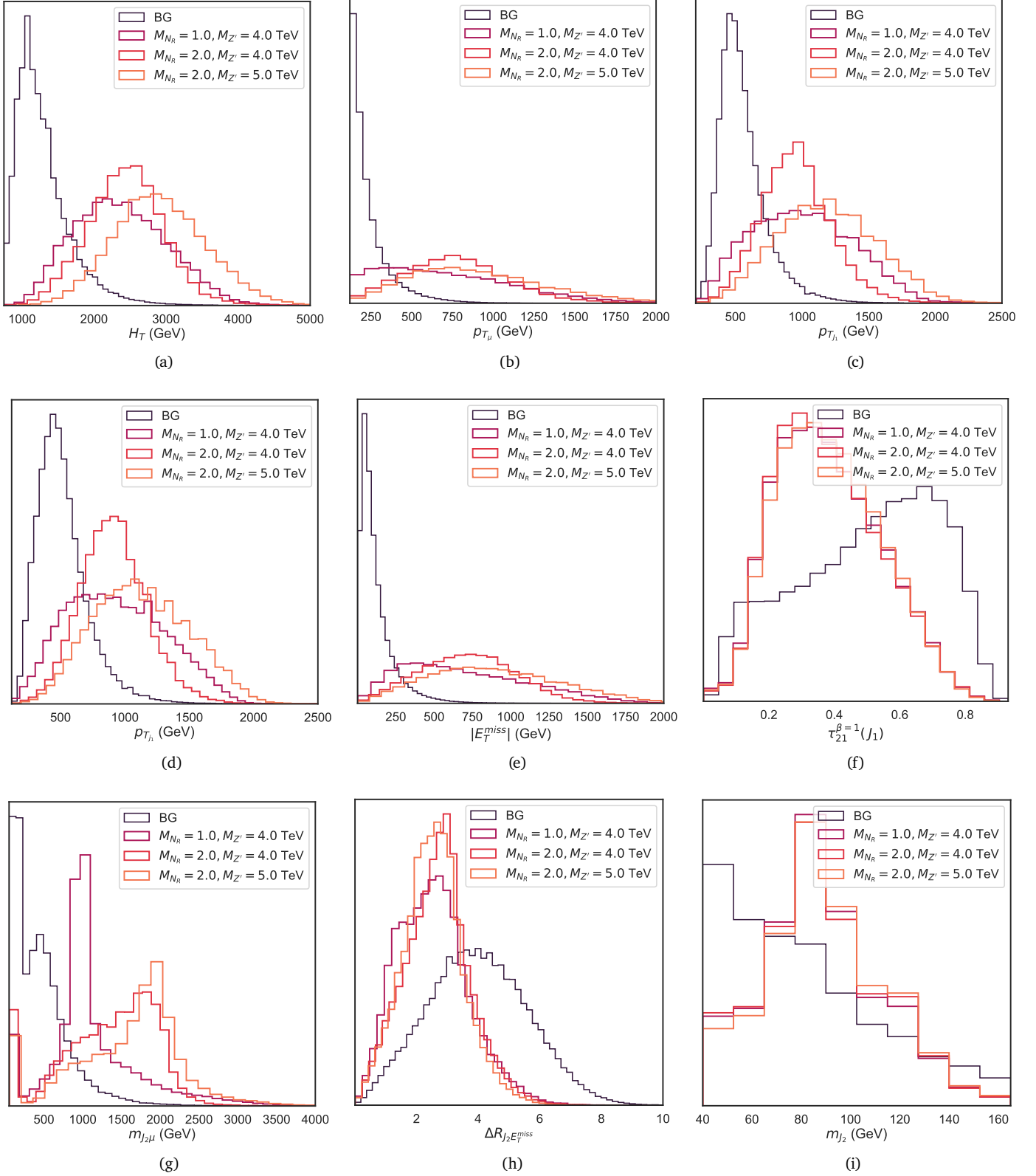


FIG. 2. Normalised density plots of the key features after passing through the cuts \mathcal{C}_1 to \mathcal{C}_5 for three benchmark points: (a) $M_{N_R} = 1$, $M_{Z'} = 4.0$ TeV, (b) $M_{N_R} = 2.0$, $M_{Z'} = 4.0$ TeV and (c) $M_{N_R} = 2.0$, $M_{Z'} = 5$ TeV. Here, the fatjets are mass-ordered and the jets are p_T -ordered.

TABLE IV. Projected number of events at the 14 TeV HL-LHC at different stages of analysis in the monolepton channel for $M_{N_R} = 2$ TeV, $M_{Z'} = 5$ TeV, and $g_z = 0.3$. For the signal, we assume a K factor of 1.3 [46].

	Signal	$t_h t_\ell$	$t_\ell t_\ell$	$W_\ell + j$	$W_\ell W_h + j$	$Z_h W_\ell + j$	S/B
Initial	478	276832	4382	392206	291684	22729	4.84×10^{-4}
\mathcal{C}_1	476	262336	4035	379874	284631	22168	4.99×10^{-4}
\mathcal{C}_2	378	165438	1006	271623	209486	16168	5.70×10^{-4}
\mathcal{C}_3	375	164646	964	257573	205999	15973	5.81×10^{-4}
\mathcal{C}_4	309	101562	711	105221	99886	7559	9.81×10^{-4}
\mathcal{C}_5	308	96071	683	98984	94865	7171	1.03×10^{-3}
DNN	299	~ 11	~ 1	~ 136	~ 213	~ 15	0.8

z_u and z_d for the six different E_6 embeddings and the GS model in Table III. Between the two colour-singlet isosinglets in Table II, we identify the one with higher absolute $U(1)_z$ charge with the RHN, i.e., $z_N = \text{Max}(z_\nu, z_{\bar{\nu}})$.

We use FEYNRULES [47] to build the above model and obtain the Universal FeynRules Output (UFO). We simulate the hard scattering in MADGRAPH5 [48], showering and hadronisation in PYTHIA [49] and the LHC detector environment in DELPHES3 [50]. The events are generated at $\sqrt{s} = 14$ TeV. Jets are clustered using the anti- k_T algorithm [51] with $R = 0.4$ (we call them AK-4 jet). For the electron, the DeltaRMax parameter in the DELPHES card (distance between the other isolated objects and the identified electron) for isolation has been modified to 0.2 from 0.5.

A. Event selection criteria: Monolepton channel

We show the signal topology in Fig. 1. In Ref. [24], we performed a cut-based analysis of the dilepton signature.

TABLE V. Kinematic variables chosen to analyse the monolepton signature; τ 's are the n-subjettiness ratios.

Variable	Description
H_T	Sum of transverse momenta of hadronic objects.
p_{T_i}	Transverse Momenta of all reconstructed objects.
\cancel{E}_T	Missing transverse energy.
m_{J_i}	Invariant Masses of the reconstructed fatjets.
ΔR_{ik}	Distances between any two reconstructed objects.
$m_{J,\mu}$	Invariant masses of the fatjet-lepton pairs.
$m_{j,jk}$	Invariant masses of any two reconstructed AK-4 jets.
$\tau_{21}^{\beta=1}$	τ_2/τ_1 , $\beta = 1.0$ for each fatjet.
$\tau_{21}^{\beta=2}$	τ_2/τ_1 , $\beta = 2.0$ for each fatjet.
$\tau_{32}^{\beta=1}$	τ_3/τ_2 , $\beta = 1.0$ for each fatjet.
$\tau_{32}^{\beta=2}$	τ_3/τ_2 , $\beta = 2.0$ for each fatjet.

Here, in this paper, we mainly focus on the monolepton signature, which arises when one of the RHNs decays to a hadronically decaying W boson and a lepton (muon) while the other decays to a Z/H boson and a neutrino:

$$pp \rightarrow Z' \rightarrow N_R N_R \rightarrow \mu + \cancel{E} + \text{jets}.$$

As explained earlier, probing the monolepton channel is more challenging than the dilepton case as the backgrounds (see Table IV) are harder to tame with simple kinematic cuts. Hence, we employ a DNN model to enhance the signal sensitivity. We look at Z' masses between 3 – 7 TeV and RHNs ranging from 0.5 to 3.5 TeV. From the topology and the distributions of the final state, we design the following basic selection criteria for the signal events:

- \mathcal{C}_1 : $H_T > 750$ GeV, where H_T is the scalar sum of the transverse momenta of all hadronic objects in an event.
- \mathcal{C}_2 : Exactly one muon, with $p_T > 120$ GeV with $|\eta| < 2.5$. (We consider the muon as it has the best detector sensitivity among the leptons.)
- \mathcal{C}_3 : At least two AK-4 jets. We also demand that the leading jet has $p_T > 120$ GeV and the subleading one has $p_T > 40$ GeV.
- \mathcal{C}_4 : Exactly two fatjets, clustered using the anti- k_T algorithm with $R = 0.7$ and $p_T > 200$ GeV with mass $M_J \in [40, 165]$.
- \mathcal{C}_5 : The invariant mass between the reconstructed muon and missing transverse energy (\cancel{E}_T) must be greater than 140 GeV, i.e., $M_{\mu\cancel{E}_T} > 140$ GeV.

We pick the fatjet radius $R = 0.7$ after optimising to tag a boosted two-pronged jet. The constraints on fatjet mass (\mathcal{C}_4) are chosen to include reconstructed W , Z and H fatjets. Since the missing energy and muon come from the decay of W -boson in all the backgrounds, we put a high cut on the invariant mass of reconstructed lepton and missing transverse energy pair in \mathcal{C}_5 .

B. Background processes

The major backgrounds considered for the analysis are listed in Table IV, along with the cut efficiencies and the total number of events at the HL-LHC luminosity, 3 ab^{-1} . We generate the background events with some generation-level cuts to reduce the computation time. The $W^\pm + jets$ process is the leading background before the cuts; the demand of a high- p_T jet (\mathcal{C}_3) and two fatjets (\mathcal{C}_4) reduces this background significantly. The contributions from the $W^+W^- + jets$ process drop drastically with the demand of two fatjets (\mathcal{C}_4). The fatjet criterion (\mathcal{C}_4) also cuts the $t\bar{t} + jets$ background as most of these events have just one fatjet. The hadronically-decaying top is sometimes reconstructed as the fatjet in a fraction of $t\bar{t} + jets$ events; the demand on the fatjet mass cuts down these events. After the event selection criteria are enforced, $W^+W^- + jets$ and $t\bar{t} + jets$ become the leading backgrounds.

C. Kinematic picture and the Deep Learning model

We use the kinematic information of the identified objects, i.e., one muon, three AK-4 jets, and two fatjets, along with some derived quantities to create the input set of variables for the multivariate analysis—the complete list of variables is given in Table V where J is used to denote a fatjet whereas j is used to identify an AK-4 jet.

We show the distributions of the key features of the signal and the background for three benchmark parameters in Fig. 2. The H_T (scalar sum of all hadronic objects) distributions show a clear separation between the signals and background due to the boosted nature of the final state; see Fig. 2(a). Moreover, for the signals, the transverse momentum distributions of the tagged muon, AK-4 jets, and the fatjet and the \cancel{E}_T distribution peak at considerably higher values than those of the background, see Figs. 2(b), 2(c), 2(d), 2(e). We also consider the n -subjettiness variables [52] which check for two-pronged (τ_2/τ_1) and three-pronged (τ_3/τ_2) nature of a fatjet for various values of β ($\beta \in \{1, 2, 3\}$). Since our fatjet parameters are tuned to identify a W -like (two-pronged) jet, the τ_2/τ_1 ratios are the key variables. Of these, the τ_2/τ_1 for $\beta = 2$ gives a clear separation between the signals and the background [Fig. 2(f)]. The τ_3/τ_2 ratios do not offer clear separations, but, nevertheless, we include them due to the inclusive nature of the analysis cuts on the number of fatjets. The variable $m_{J_i\ell}$ (invariant mass of a fatjet and the tagged muon) reconstructs the mass of the RHN very well—the trend can be clearly seen in Fig. 2(g). The $\Delta R_{J_i\cancel{E}_T}$ distributions in Fig. 2(h) can also distinguish the signals and the background well, as the final state objects come from the decay of an on-shell Z' . From the full set of kinematic variables, we drop the features that offer little separation between the signals and the background. For instance, we ignore the features $\Delta R_{J_1j_1}$ and $\Delta R_{J_2j_2}$ as we see that the leading (subleading) jet gets clustered inside the leading

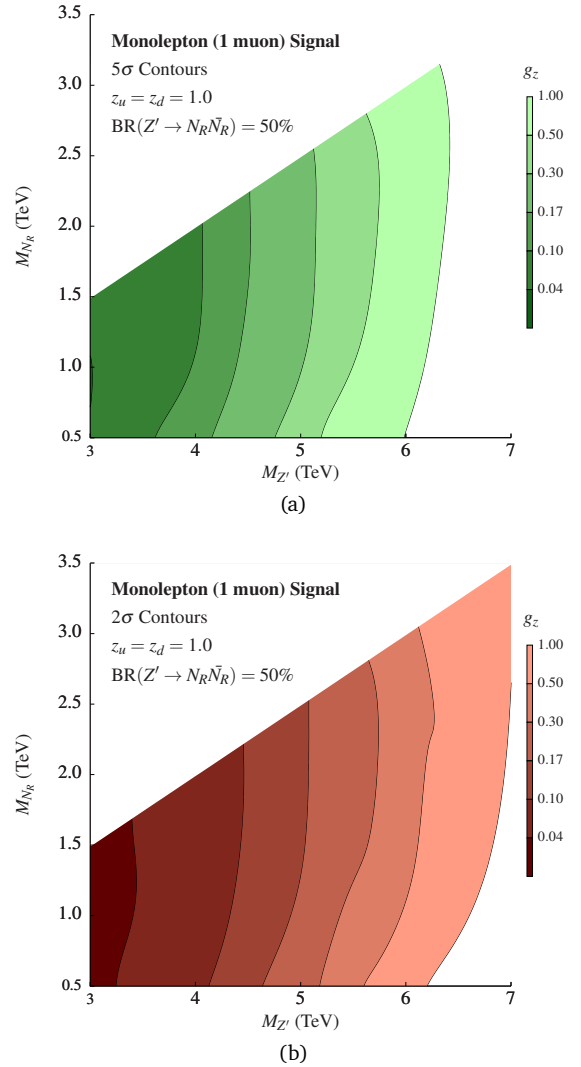


FIG. 3. The (a) discovery (5σ) and (b) exclusion ($\sim 2\sigma$) contours for the monolepton (1-muon) channel of $pp \rightarrow Z' \rightarrow N_R N_R$.

(subleading) fatjet for both signal and backgrounds. We also drop $\Delta R_{j_2j_3}$, $m_{j_1j_3}$ and $m_{j_2j_3}$ as they show overlapping signal and background distributions.

To perform the classification task, we use a fully connected DNN model with an input layer, four hidden layers (with 50, 35, 30, and 10 nodes in the layers, respectively) and a single output layer. We implement the network using the TensorFlow module [53] and use a binary cross-entropy loss and the AdamW optimiser [54] with a learning rate 0.001 to train the network. We pick the benchmark point $(M_{Z'}, M_{N_R}) = (5.0, 2.0)$ TeV to optimise the hyperparameters using a grid search. The performance metric is the signal significance (\mathcal{S} score),

$$\mathcal{S} = \sqrt{2(N_S + N_B) \ln \left(\frac{N_S + N_B}{N_B} \right)} - 2N_S, \quad (14)$$

where N_S and N_B are the numbers of signal and background events the network allows at 3 ab^{-1} luminosity.

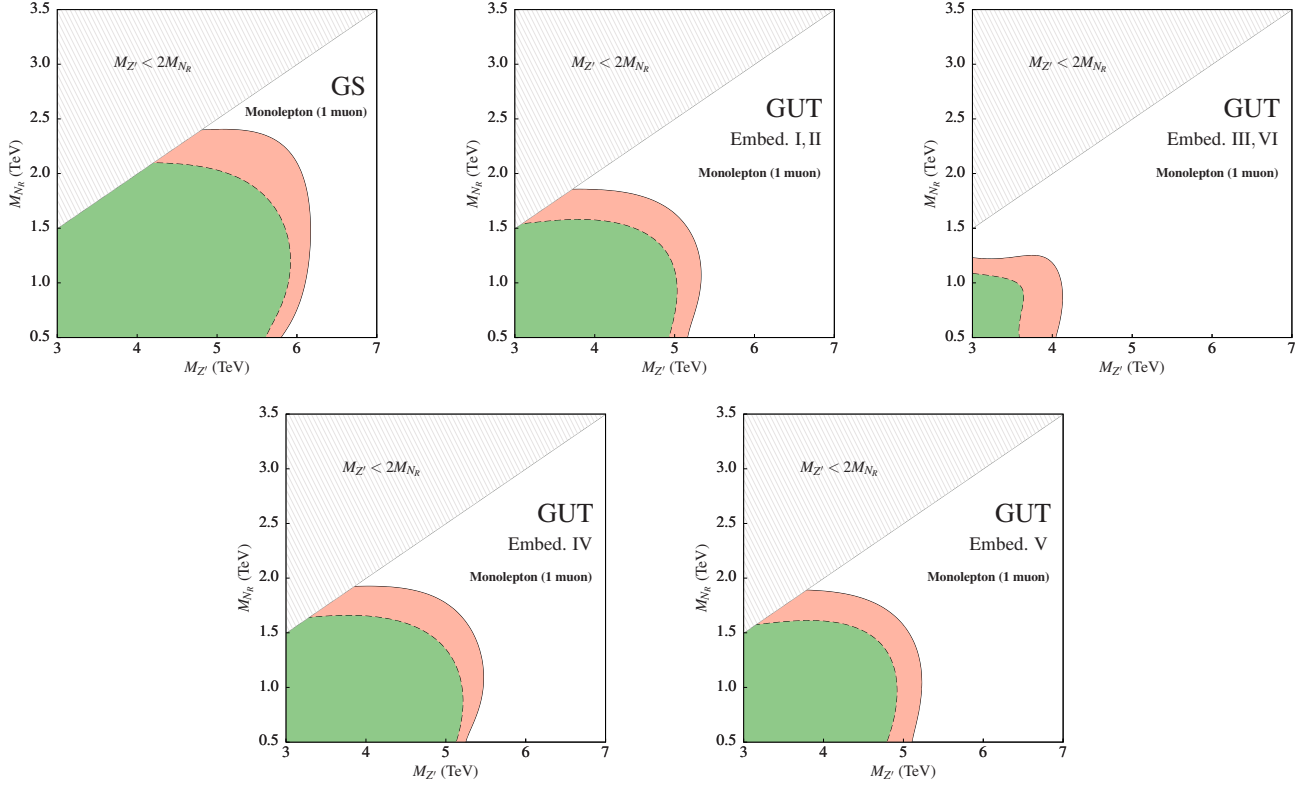


FIG. 4. HL-LHC reaches for the GS model and the E_6 embeddings in the monolepton channel for $g_z = 0.72$. The green regions (dotted contours) are discoverable (5σ), and the red regions are excludable (2σ). The $U(1)_z$ charges are found in Table III .

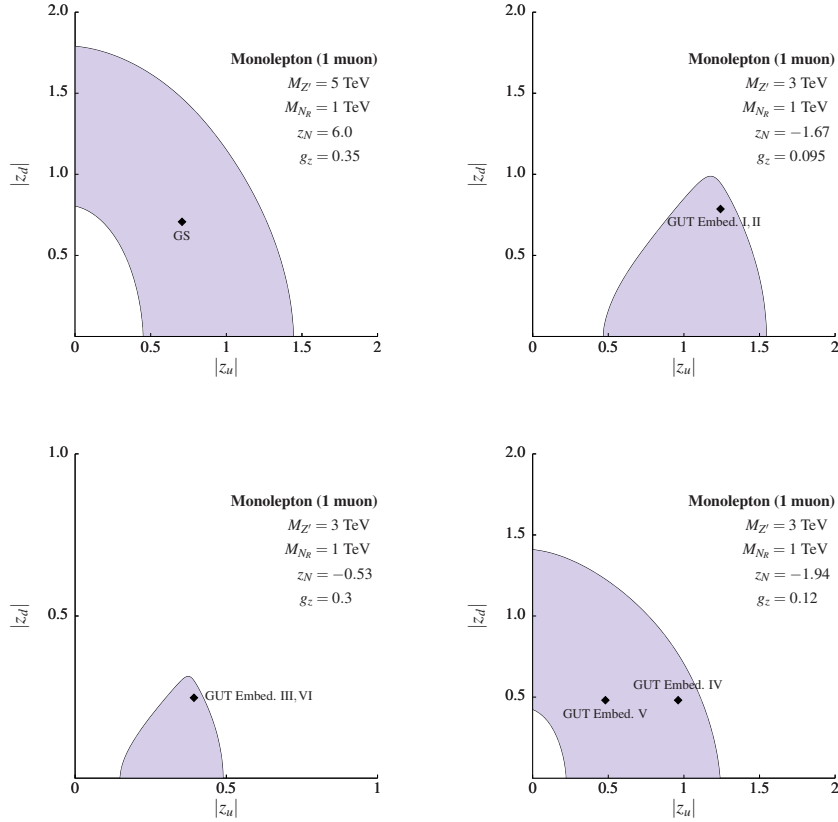


FIG. 5. Regions where the monolepton signal achieves at least 2σ significance at the HL-LHC but are beyond the projected reach in the dijet channel (see text).

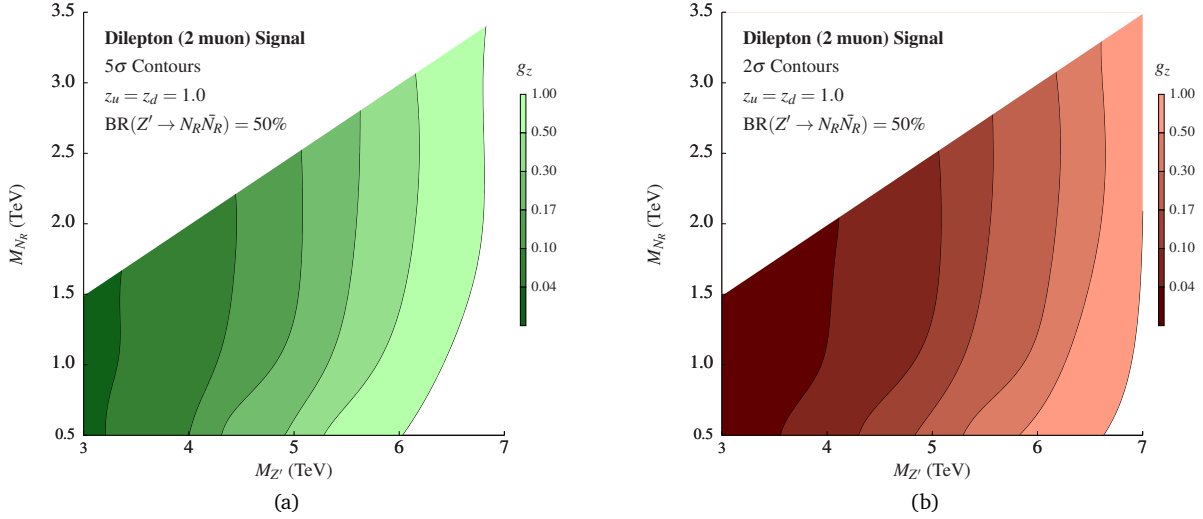


FIG. 6. The (a) discovery (5σ) and (b) exclusion ($\sim 2\sigma$) contours for the dilepton (2-muon) channel of $pp \rightarrow Z' \rightarrow N_R N_R$.

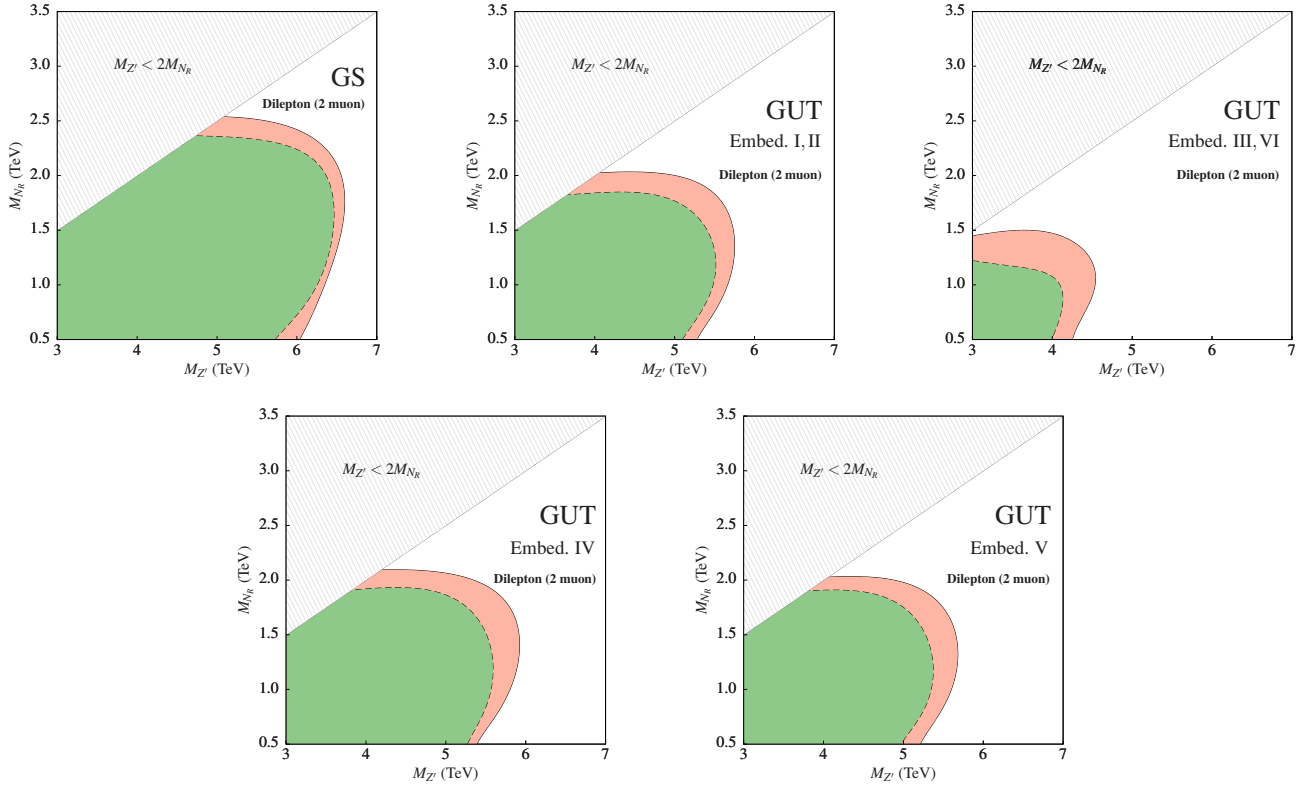


FIG. 7. HL-LHC reaches for the GS model and the E_6 embeddings in the dilepton channel for $g_z = 0.72$. The green regions (dotted contours) are discoverable (5σ), and the red regions are excludable (2σ). The $U(1)_z$ charges are found in Table III .

IV. MONOLEPTON CHANNEL PROSPECTS

Fig. 3 shows the HL-LHC discovery (5σ) and exclusion ($\sim 2\sigma$) reaches through the monolepton channel in a model-independent manner. Assuming a fixed $\text{BR}(Z' \rightarrow N_R N_R) = 50\%$, we mark the contours of the $U(1)_z$ gauge coupling, g_z [Eq. (2)], needed to achieve 5σ and 2σ significances on the $M_{Z'} - M_{N_R}$ plane. To calculate the number of events,

N_S and N_B , we have used the final efficiencies of the DNN model at the working point with DNN response = 0.95. The g_z contours are broadly insensitive to the mass of the RHN. However, because of the high boosts, the event selection efficiency around $M_{N_R} = 0.5$ TeV (or less) is lower than those at larger values. Hence, one needs a larger g_z to achieve a high signal significance. This can be seen from the slightly deformed contours between $M_{N_R} = 1.0$ TeV and $M_{N_R} = 0.5$

TeV.

In particular models, however, the Z' BR will not be fixed. For example, in Fig. 4, we show the 5σ and 2σ contours for the GS model and the six E_6 embeddings for $g_z = 0.72$ ($\approx g_{ew}$); the corresponding $U(1)_z$ charges are found in Table III. As the $M_{N_R}/M_{Z'}$ ratio approaches the threshold value, $1/2$, $\text{BR}(Z' \rightarrow N_R N_R)$ drops. This is why the contours in Fig. 4 turn inwards with increasing M_{N_R} near the kinematic threshold (top-left edge).

In Fig. 5, we show the regions that will be beyond the reach of the dijet channel at the HL-LHC (approximately) but can be reached ($\gtrsim 2\sigma$) by the monolepton signal. To estimate the projected dijet reach, we have simply scaled down the current ATLAS dijet exclusion limits by the square root of the luminosity ratio ($\sqrt{3000/140} \approx 4.65$), ignoring the difference between the centre-of-mass energies.

V. UPDATE: DILEPTON CHANNEL PROSPECTS

We update our earlier cut-based estimates of the dilepton prospects [24] with the current DNN model. The dileptonic signal comes from the following process,

$$pp \rightarrow Z' \rightarrow N_R N_R \rightarrow (W^+ \mu^-) (W^- \mu^-), \quad (15)$$

where the W bosons decay hadronically. See Ref. [24] for a discussion on the important background processes. The event-selection criteria remain similar to those in Sec. III A with some minor changes: in \mathcal{C}_2 , we now demand two muons with $p_T > 120$ GeV and the new fatjet window in \mathcal{C}_4 is now $[40, 120]$ to only tag W -like fatjets. To suppress the huge Drell-Yan dilepton background, a Z -veto cut is necessary; we also change \mathcal{C}_5 to demand that the invariant mass of the muon pair ($m_{\ell\ell}$) be greater than 140 GeV.

We show the model-independent HL-LHC discovery (5σ) and exclusion ($\sim 2\sigma$) reaches through the dilepton channel in Fig. 6 and the 5σ and 2σ contours for the GS model and the six E_6 embeddings with $g_z = 0.72$ in Fig. 7. Comparing Fig. 6 with Fig. 4 of Ref. [24], we see the DNN has enhanced the reaches (discovery and exclusion) significantly.

VI. CONCLUSIONS

In this paper, we studied the prospects of a correlated search of a heavy neutral gauge boson Z' and the right-handed neutrino N_R in leptophobic $U(1)$ extensions. In particular, we analysed an experimentally unexplored channel $pp \rightarrow Z' \rightarrow N_R N_R$ where the N_R pair decays to a monomuon final state. While in Ref. [24] we only considered the GS model and the standard E_6 embedding, here, we study all possible embeddings of E_6 GUT models where a leptophobic Z' can dominantly decay to TeV-scale RHNs in large parts of the parameter space. Moreover, unlike the dilepton signature considered in our previous paper [24], probing the monolepton signature is highly challenging due to the huge background from the SM processes, which are hard to reduce with a cut-based analysis. Hence, in this paper, we used a DNN model to isolate the signal from the SM background, providing orders of magnitude gains in significance scores. With this, we found both mono and dilepton channels to be comparable and highly promising; for order electroweak coupling (g_z), a Z' with mass up to $6 - 7$ TeV can be discovered at the 14 TeV HL-LHC. Therefore, this follow-up paper improves upon our previous study on several counts: it covers more model possibilities with a more sophisticated analysis. It also covers the complementary signatures—mono and dilepton channels—to present a comprehensive view of the prospects of this exciting but experimentally unexplored process.

VII. ACKNOWLEDGEMENTS

We thank T. Rizzo for insightful discussions on the E_6 embeddings. C. N. acknowledges the Department of Science and Technology (DST)-Inspire for his fellowship. We also thank Jai Bardhan for helping us speed up the input-feature generation pipeline and for helpful discussions.

-
- [1] P. Langacker, *Grand Unified Theories and Proton Decay*, *Phys. Rept.* **72** (1981) 185.
 - [2] D. London and J. L. Rosner, *Extra Gauge Bosons in $E(6)$* , *Phys. Rev. D* **34** (1986) 1530.
 - [3] J. L. Hewett and T. G. Rizzo, *Low-Energy Phenomenology of Superstring Inspired $E(6)$ Models*, *Phys. Rept.* **183** (1989) 193.
 - [4] A. Leike, *The Phenomenology of extra neutral gauge bosons*, *Phys. Rept.* **317** (1999) 143–250, [[hep-ph/9805494](#)].
 - [5] P. Langacker, *The Physics of Heavy Z' Gauge Bosons*, *Rev. Mod. Phys.* **81** (2009) 1199–1228, [[0801.1345](#)].
 - [6] ATLAS collaboration, G. Aad et al., *Search for new resonances in mass distributions of jet pairs using 139 fb^{-1} of pp collisions at $\sqrt{s} = 13 \text{ TeV}$ with the ATLAS detector*, *JHEP* **03** (2020) 145, [[1910.08447](#)].
 - [7] CMS collaboration, A. M. Sirunyan et al., *Search for high mass dijet resonances with a new background prediction method in proton-proton collisions at $\sqrt{s} = 13 \text{ TeV}$* , *JHEP* **05** (2020) 033, [[1911.03947](#)].
 - [8] ATLAS collaboration, G. Aad et al., *Search for high-mass dilepton resonances using 139 fb^{-1} of pp collision data collected at $\sqrt{s} = 13 \text{ TeV}$ with the ATLAS detector*, *Phys. Lett. B* **796** (2019) 68–87, [[1903.06248](#)].
 - [9] CMS collaboration, A. M. Sirunyan et al., *Search for resonant and nonresonant new phenomena in high-mass dilepton final states at $\sqrt{s} = 13 \text{ TeV}$* , *JHEP* **07** (2021) 208, [[2103.02708](#)].
 - [10] ATLAS collaboration, M. Aaboud et al., *Search for*

resonances in diphoton events at $\sqrt{s}=13$ TeV with the ATLAS detector, *JHEP* **09** (2016) 001, [[1606.03833](#)].

- [11] CMS collaboration, V. Khachatryan et al., Search for high-mass diphoton resonances in proton–proton collisions at 13 TeV and combination with 8 TeV search, *Phys. Lett. B* **767** (2017) 147–170, [[1609.02507](#)].
- [12] ATLAS collaboration, G. Aad et al., Search for heavy diboson resonances in semileptonic final states in pp collisions at $\sqrt{s} = 13$ TeV with the ATLAS detector, *Eur. Phys. J. C* **80** (2020) 1165, [[2004.14636](#)].
- [13] CMS collaboration, A. Tumasyan et al., Search for heavy resonances decaying to WW, WZ, or WH boson pairs in the lepton plus merged jet final state in proton-proton collisions at $\sqrt{s} = 13$ TeV, *Phys. Rev. D* **105** (2022) 032008, [[2109.06055](#)].
- [14] CMS collaboration, V. Khachatryan et al., Search for resonant $t\bar{t}$ production in proton-proton collisions at $\sqrt{s} = 8$ TeV, *Phys. Rev. D* **93** (2016) 012001, [[1506.03062](#)].
- [15] A. Ferrari, Study of the production of a new Z' boson and its decay into Majorana neutrinos in pp collisions at $s = 14$ -TeV and in e^+e^- collisions at $s = 3$ -TeV, *Phys. Rev. D* **65** (2002) 093008.
- [16] A. Das, N. Okada and D. Raut, Enhanced pair production of heavy Majorana neutrinos at the LHC, *Phys. Rev. D* **97** (2018) 115023, [[1710.03377](#)].
- [17] A. Das, N. Okada and D. Raut, Heavy Majorana neutrino pair productions at the LHC in minimal $U(1)$ extended Standard Model, *Eur. Phys. J. C* **78** (2018) 696, [[1711.09896](#)].
- [18] P. Cox, C. Han and T. T. Yanagida, LHC Search for Right-handed Neutrinos in Z' Models, *JHEP* **01** (2018) 037, [[1707.04532](#)].
- [19] G. Chauhan and P. S. B. Dev, Interplay between resonant leptogenesis, neutrinoless double beta decay and collider signals in a model with flavor and CP symmetries, *Nucl. Phys. B* **986** (2023) 116058, [[2112.09710](#)].
- [20] A. Das, S. Mandal, T. Nomura and S. Shil, Heavy Majorana neutrino pair production from Z' at hadron and lepton colliders, *Phys. Rev. D* **105** (2022) 095031, [[2202.13358](#)].
- [21] A. Ekstedt, R. Enberg, G. Ingelman, J. Löfgren and T. Mandal, Constraining minimal anomaly free $U(1)$ extensions of the Standard Model, *JHEP* **11** (2016) 071, [[1605.04855](#)].
- [22] G. K. Leontaris and J. Rizos, New fermion mass textures from anomalous $U(1)$ symmetries with baryon and lepton number conservation, *Nucl. Phys. B* **567** (2000) 32–60, [[hep-ph/9909206](#)].
- [23] A. Ekstedt, R. Enberg, G. Ingelman, J. Löfgren and T. Mandal, Minimal anomalous $U(1)$ theories and collider phenomenology, *JHEP* **02** (2018) 152, [[1712.03410](#)].
- [24] M. T. Arun, A. Chatterjee, T. Mandal, S. Mitra, A. Mukherjee and K. Nivedita, Search for the Z' boson decaying to a right-handed neutrino pair in leptophobic $U(1)$ models, *Phys. Rev. D* **106** (2022) 095035, [[2204.02949](#)].
- [25] D. Choudhury, K. Deka, T. Mandal and S. Sadhukhan, Neutrino and Z' phenomenology in an anomaly-free $U(1)$ extension: role of higher-dimensional operators, *JHEP* **06** (2020) 111, [[2002.02349](#)].
- [26] K. Deka, T. Mandal, A. Mukherjee and S. Sadhukhan, Leptogenesis in an anomaly-free $U(1)$ extension with higher-dimensional operators, *Nucl. Phys. B* **991** (2023) 116213, [[2105.15088](#)].
- [27] M. Thomas Arun, T. Mandal, S. Mitra, A. Mukherjee, L. Priya and A. Sampath, Testing left-right symmetry with an inverse seesaw mechanism at the LHC, *Phys. Rev. D* **105** (2022) 115007, [[2109.09585](#)].
- [28] A. Bhaskar, Y. Chaurasia, K. Deka, T. Mandal, S. Mitra and A. Mukherjee, Right-handed neutrino pair production via second-generation leptoquarks, *Phys. Lett. B* **843** (2023) 138039, [[2301.11889](#)].
- [29] R. N. Mohapatra, Mechanism for Understanding Small Neutrino Mass in Superstring Theories, *Phys. Rev. Lett.* **56** (1986) 561–563.
- [30] R. N. Mohapatra and J. W. F. Valle, Neutrino Mass and Baryon Number Nonconservation in Superstring Models, *Phys. Rev. D* **34** (1986) 1642.
- [31] D. Das, K. Ghosh, M. Mitra and S. Mondal, Probing sterile neutrinos in the framework of inverse seesaw mechanism through leptoquark productions, *Phys. Rev. D* **97** (2018) 015024, [[1708.06206](#)].
- [32] S. Jana, P. K. Vishnu and S. Saad, Minimal dirac neutrino mass models from $U(1)_R$ gauge symmetry and left–right asymmetry at colliders, *Eur. Phys. J. C* **79** (2019) 916, [[1904.07407](#)].
- [33] A. Das, S. Goswami, K. N. Vishnudath and T. Nomura, Constraining a general $U(1)'$ inverse seesaw model from vacuum stability, dark matter and collider, *Phys. Rev. D* **101** (2020) 055026, [[1905.00201](#)].
- [34] P. Bandyopadhyay, S. Jangid and M. Mitra, Scrutinizing Vacuum Stability in IDM with Type-III Inverse seesaw, *JHEP* **02** (2021) 075, [[2008.11956](#)].
- [35] A. Das, S. Goswami, V. K. N. and T. K. Poddar, Freeze-in sterile neutrino dark matter in a class of $U(1)'$ models with inverse seesaw, [2104.13986](#).
- [36] S. Banerjee, P. S. B. Dev, A. Ibarra, T. Mandal and M. Mitra, Prospects of Heavy Neutrino Searches at Future Lepton Colliders, *Phys. Rev. D* **92** (2015) 075002, [[1503.05491](#)].
- [37] S. Chakraborty, M. Mitra and S. Shil, Fat Jet Signature of a Heavy Neutrino at Lepton Collider, *Phys. Rev. D* **100** (2019) 015012, [[1810.08970](#)].
- [38] D. Barducci and E. Bertuzzo, The see-saw portal at future Higgs factories: the role of dimension six operators, *JHEP* **06** (2022) 077, [[2201.11754](#)].
- [39] K. S. Babu, C. F. Kolda and J. March-Russell, Leptophobic $U(1)$ s and the $R(b) - R(c)$ crisis, *Phys. Rev. D* **54** (1996) 4635–4647, [[hep-ph/9603212](#)].
- [40] J. L. Lopez and D. V. Nanopoulos, Leptophobic Z' in stringy flipped $SU(5)$, *Phys. Rev. D* **55** (1997) 397–406, [[hep-ph/9605359](#)].
- [41] T. G. Rizzo, Gauge kinetic mixing and leptophobic Z' in $E(6)$ and $SO(10)$, *Phys. Rev. D* **59** (1998) 015020, [[hep-ph/9806397](#)].
- [42] K. Leroux and D. London, Flavor changing neutral currents and leptophobic Z' gauge bosons, *Phys. Lett. B* **526** (2002) 97–103, [[hep-ph/0111246](#)].
- [43] P. Anastopoulos, M. Bianchi, E. Dudas and E. Kiritsis, Anomalies, anomalous $U(1)$'s and generalized Chern-Simons terms, *JHEP* **11** (2006) 057, [[hep-th/0605225](#)].
- [44] P. Anastopoulos, F. Fucito, A. Lionetto, G. Pradisi, A. Racioppi and Y. S. Stanev, Minimal Anomalous $U(1)$ -prime Extension of the MSSM, *Phys. Rev. D* **78** (2008) 085014, [[0804.1156](#)].
- [45] H. Hettmansperger, M. Lindner and W. Rodejohann, Phenomenological Consequences of sub-leading Terms in

- See-Saw Formulas*, *JHEP* **04** (2011) 123, [[1102.3432](#)].
- [46] E. Eichten, I. Hinchliffe, K. D. Lane and C. Quigg, *Super Collider Physics*, *Rev. Mod. Phys.* **56** (1984) 579–707. [Addendum: *Rev.Mod.Phys.* 58, 1065–1073 (1986)].
- [47] A. Alloul, N. D. Christensen, C. Degrande, C. Duhr and B. Fuks, *FeynRules 2.0 - A complete toolbox for tree-level phenomenology*, *Comput. Phys. Commun.* **185** (2014) 2250–2300, [[1310.1921](#)].
- [48] J. Alwall, R. Frederix, S. Frixione, V. Hirschi, F. Maltoni, O. Mattelaer et al., *The automated computation of tree-level and next-to-leading order differential cross sections, and their matching to parton shower simulations*, *JHEP* **07** (2014) 079, [[1405.0301](#)].
- [49] T. Sjöstrand, S. Ask, J. R. Christiansen, R. Corke, N. Desai, P. Ilten et al., *An introduction to PYTHIA 8.2*, *Comput. Phys. Commun.* **191** (2015) 159–177, [[1410.3012](#)].
- [50] **DELPHES 3** collaboration, J. de Favereau, C. Delaere, P. Demin, A. Giammanco, V. Lemaître, A. Mertens et al., *DELPHES 3, A modular framework for fast simulation of a generic collider experiment*, *JHEP* **02** (2014) 057, [[1307.6346](#)].
- [51] M. Cacciari, G. P. Salam and G. Soyez, *The anti- k , jet clustering algorithm*, *JHEP* **04** (2008) 063, [[0802.1189](#)].
- [52] J. Thaler and K. Van Tilburg, *Identifying Boosted Objects with N -subjettiness*, *JHEP* **03** (2011) 015, [[1011.2268](#)].
- [53] M. Abadi, A. Agarwal, P. Barham, E. Brevdo, Z. Chen, C. Citro et al., *TensorFlow: Large-scale machine learning on heterogeneous systems*, **1603.04467**. Software available from [tensorflow.org](https://www.tensorflow.org).
- [54] I. Loshchilov and F. Hutter, *Decoupled Weight Decay Regularization*, *International Conference on Learning Representations* (2019) , [[1711.05101](#)].